Article

275–305 GHz FM-CW Radar 3D Imaging for Walk-Through Security Body Scanner

Tomofumi Ikari [1,2,*], Yoshiaki Sasaki [1] and Chiko Otani [1,3]

1   RIKEN Center for Advanced Photonics, RIKEN, Sendai 980-0845, Miyagi, Japan; otani@riken.jp (C.O.)
2   Spectra Design Ltd., Otawara 324-0403, Tochigi, Japan
3   Department of Physics, Tohoku University, Sendai 980-8578, Miyagi, Japan
*   Correspondence: ikari@a.riken.jp; Tel.: +81-287-98-3066

Abstract: Imaging using millimeter waves (MMW) and terahertz (THz) waves can help inspect hazardous materials hidden beneath clothing in a non-contact and non-invasive manner. A 3D terahertz imaging system for security gate applications in the 275–305 GHz range was developed and experimentally demonstrated to detect concealed objects carried by pedestrians. This system performs 3D measurements by combining depth detection using frequency-modulated continuous wave (FM-CW) radar, vertical scanning of the detection spot using a 1D high-speed mechanical beam scanner, and horizontal movement of the irradiated area and detection spot as the pedestrian walks. The high-speed beam scanner comprises an F-Theta telecentric lens and a polygon mirror. It has a vertical line scan rate of 142 lines/s and spatial resolution of ~10 mm, consistent with the design value, and a depth resolution of ~7 mm, which is 40% larger than the theoretical value estimated from the FM-CW radar principle. The depth-dependent lateral distortion in 3D images, known as telecentricity, measured using the body scanner imaging system, was also evaluated. Consequently, images with the same magnification were obtained at a range of more than 500 mm of focus depth. Finally, the detection of concealed objects carried by pedestrians was demonstrated, showing that the system can work for a pedestrian walking at speeds from 4 km/h to 7 km/h.

Keywords: FM-CW radar; 3D imaging; security body scanner

1. Introduction

Imaging using millimeter waves (MMW) and terahertz (THz) waves demonstrates good transparency for non-metallic materials and moderate spatial resolution in imaging, and can help detect hazardous materials hidden beneath clothing in a non-contact and non-invasive manner [1]. Active transmission imaging systems using MMWs have been installed at security gates in many airports [2]. However, this system is stationary, images a passenger at a specific posture, and requires approximately 10 s of screening time per passenger. For example, at crowded train gates and event entrances, security inspections of more than several thousand people per hour must be performed without stopping the flow of people, and it is desirable to introduce walk-through body scanners that can inspect for concealed objects while walking. Moreover, the active method is advantageous to obtain sufficient measurement accuracy in a short time using a room temperature system that does not require a cryogenic cooling system. Furthermore, the contrast between reflected signals from the human body and hazardous materials is not sufficient in 2D intensity images obtained by active imaging with MMWs and THz waves [1]. Therefore, in concealed object detection, the 3D shape must be measured under the garment.

One way of achieving this objective is using 3D radar imaging technology; however, the challenge in using this technology for walk-through body scanners is to reduce the measurement time. The 3D measurement must be completed within a few seconds of a pedestrian passing through the gate. However, 3D radar measurement requires depth

direction (range direction) measurement at each irradiation point, increasing the measurement time. To solve this problem, the development of arrays of subharmonic heterodyne detector elements and high-speed 2D beam scanners has been considered [3–9]. However, this can create new problems, such as increased complexity in system configuration, data processing, and increased system costs.

To make the system as simple and inexpensive as possible, it is desirable to realize an inspection system using a single-element transmitter and receiver. Therefore, we propose a new THz wave 3D imaging measurement method that is specialized for security gate applications and can realize a walk-through body scanner using a single transmitter and receiver. The system combines depth detection by frequency-modulated continuous wave (FM-CW) radar, vertical scanning of the detection spot by a 1D high-speed mechanical beam scanner, and movement of the illuminated area and detection spot as the pedestrian walks to make 3D measurements. This configuration minimizes the number of beam scan axis required to measure a pedestrian and enables a 3D image measurement of the human body in the time it takes for a pedestrian to pass. The only mechanical beam scan is the vertical scanning of the detection beam using a polygon mirror and an F-Theta telecentric lens [10–13].

In this system, the 300 GHz band was adopted due to the following reasons. The attenuation of cloth fibers increases with increasing frequency and is less than -3 dB below 300 GHz [14]. On the other hand, a higher frequency is better in order to realize the better spatial resolution of acquired images. Thus, the 300 GHz band is suitable for our purpose. Moreover, the recent progress toward Beyond 5G/6G will lead to the tremendous reduction of cost for the devices in this band in the near future.

In this study, we present the measurement concept and system configuration of our walk-through body scanner, the evaluation of its optical characteristics, and the results of high-speed imaging of a pedestrian.

2. Concept and Configuration

2.1. Measurement Concept and System Overview

To maintain the flow of pedestrians at the security gate, the system must be placed such that it does not obstruct walking. Therefore, this system irradiates THz waves at an angle of 45° to the direction of walking and detects the reflected and scattered waves. Figure 1 shows the system concept. The final system consists of three to four small identical units stacked vertically, as shown in Figure 1, to obtain 3D images of a pedestrian from the front, back, and both left and right sides. Each unit covers an area of approximately 30 cm high, and it is assumed that imaging data from each unit is combined to reconstruct the entire image. Here, a prototype unit was constructed.
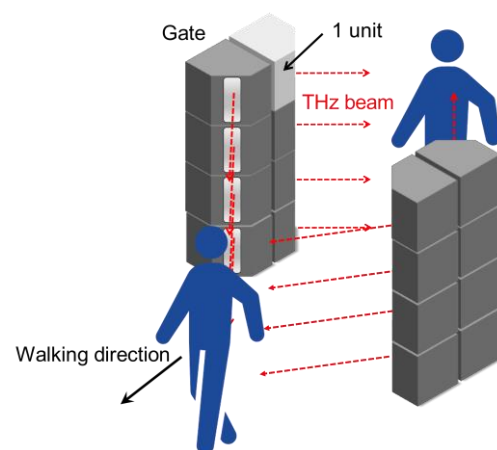

Figure 1. Concept diagram of walk-through body scanner.

The system uses a transceiver comprising a single transmitter and receiver pair, and beam scanning is required to acquire a 3D image. However, the more beam scans are required, the longer the measurement time is. To solve this, this system employs an imaging method that utilizes pedestrian walking and radar measurements, which reduces the measurement time by decreasing the mechanical scanning to a single axis and realizes walk-through measurement at an actual walking speed.

Figure 2a shows an overview of the measurement from above. As the pedestrian moves forward, the irradiated area moves from the left half of the body to the right half. Figure 2b is a conceptual view of the pedestrian from the front, where the detection spot is scanned vertically by a mechanical beam scanner, which will be described later.
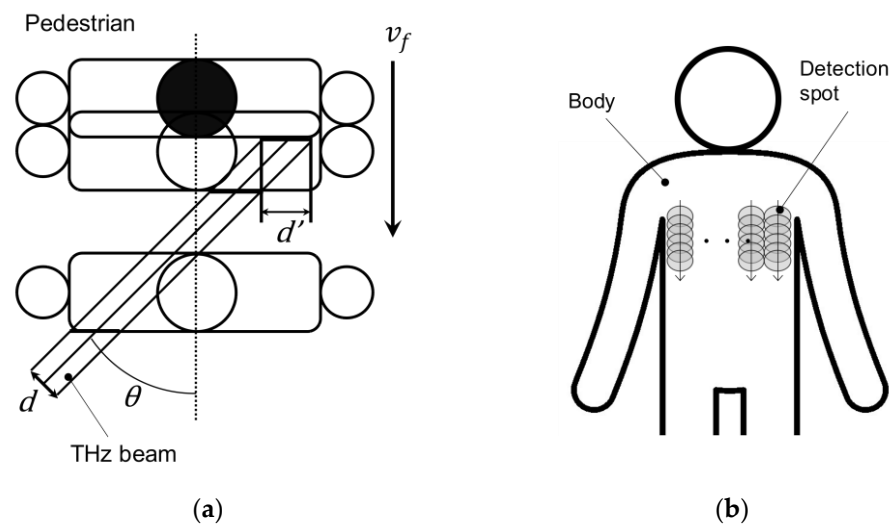

(**a**) (**b**)

Figure 2. (**a**) Conceptual view of the measurement from above. (**b**) A conceptual view of the pedestrian from the front.

For the detection spot to cover the entire inspection area with this method, it should be scanned vertically at a faster speed than the walking speed. Specifically, the time required to vertically scan the detection spot (t_s) should be shorter than that required for the detection spot to move horizontally by the width of the diameter of the spot (t_d) owing to walking. Therefore, when the diameter of the detection spot is d, the detection spot diameter at the human body surface is d', the angle of incidence is θ, and walking speed is v_f,

$$t_s \leq t_d = \frac{d'}{v_f} = \frac{d}{v_f \, \sin(\theta)}. \tag{1}$$

This unit was designed with v_f = 3.6 km/h, d = 10 mm, and an irradiation angle θ of 45°. Applying these conditions to Equation (1), the time for the detection spot to move horizontally by its diameter, t_d, is calculated as 14.1 ms; thus, the time for one vertical scan period, t_s, should be shorter than this. Moreover, because the actual walking speed is approximately 1 m/s, the beam scan should be performed at twice the speed of the torso to evenly image the legs that move during walking. Based on these conditions, the period t_s of the vertical scan was set to 7.1 ms, half the period of t_d. This corresponds to a vertical scan rate of 142 lines/s for the detection beam.

In addition, any walk-through body scanner requires that the measurement not be interrupted by other pedestrians walking in front of the pedestrian. This system also requires that the distance between pedestrians be kept so that the image is not obscured. On the other hand, when a terahertz wave is illuminated from a 45° angle, as in our system, the measurements can be performed continuously and at high speed as long as the distance between pedestrians is maintained, unlike when the measurements are performed from the front. The actual distance required in our system is well over the width of a person,

about 0.5–1 m. This is feasible enough since security inspectors usually involve walking in turn in a line.

A photograph of the developed walk-through body scanner is shown in Figure 3. The main unit of the scanner is $695 \times 465 \times 905$ mm, which is installed on an elevating platform. Pedestrians walk between gate sensors 1 (GS1) and 2 (GS2) from the back to the front. The distance between gates is approximately 1 m, and the pedestrian passes through in 1 s when walking at a speed of 3.6 km/h (1 m/s). The 3D image appears on the display 0.4 s after a pedestrian passes through GS2, and then, the next pedestrian can be scanned.
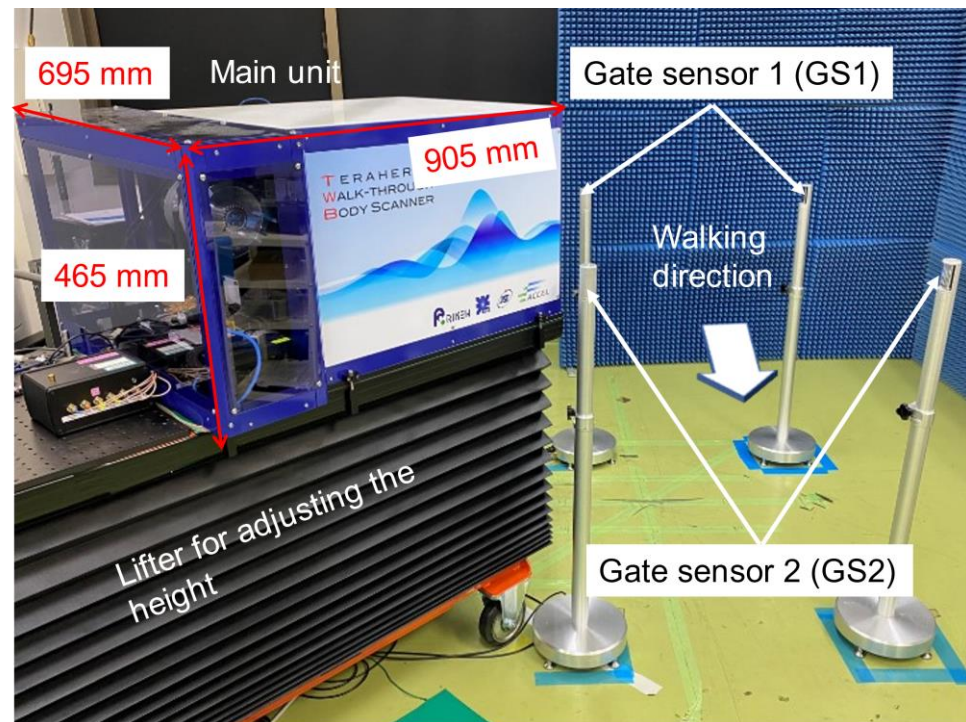

Figure 3. Photograph of our walk-through body scanner.

2.2. FM-CW Radar Subsystem

The body scanner uses a single transceiver with an output of 30 mW and a frequency sweep rate of 3 GHz/µs in the 275–305 GHz range. To evaluate the effective dynamic range, we have performed the measurements by adding multiple attenuators to the transmitter and determined the minimum detectable power. Then, the ratio of the maximum output power to the minimum sensitivity was 110 dB for the transceiver.

Figure 4 shows the transceiver used for the body scanner. It consists of a frequency synthesizer in the 12 GHz band, a 300 GHz transmitter (Tx) using a frequency multiplier chain, and a subharmonic mixer as the receiver (Rx). This multiplier chain was developed by ACST GmbH, Hanau, Germany. In the synthesizer, a direct digital synthesizer (DDS) generates a frequency-modulated signal at 424.4–470.7 MHz, and the signal is multiplied by 27 to produce microwaves in the 11.46–12.71 GHz range. The synthesizer was developed by SYSTECRESEARCH Inc. Co. Ltd., Sagamihara, Japan. The signal is inputted into the transceiver and multiplied by 12 by the multiplier chain to produce a 137.5–152.5 GHz signal. This signal is divided into two parts, one of which is further multiplied by 2 to produce a Tx signal, and the other is input to the subharmonic mixer as a local oscillator (LO) signal of Rx. A diagonal horn antenna is coupled to the signal output of Tx, and a similar antenna is also used at the input of Rx. At Rx, the received and LO signals are input to a subharmonic mixer to generate an intermediate frequency (IF) signal with a differential

frequency of Δf, which is then it is amplified and output by an IF low noise amplifier. Δf is expressed as follows:

$$\Delta f = \frac{2\beta R}{c} \qquad (2)$$

where β is the frequency sweep rate, R is the distance from the transceiver to the target, and c is the speed of light. Because R = 1.5–2.5 m was assumed in this system, the IF frequency range was 30–50 MHz for β = 30 GHz/10 µs. The depth ("range") resolution, ΔR, is expressed as follows:

$$\Delta R = \frac{c}{2B} \qquad (3)$$

where B is the sweep frequency bandwidth, and ΔR was 5 mm for B = 30 GHz in our system.
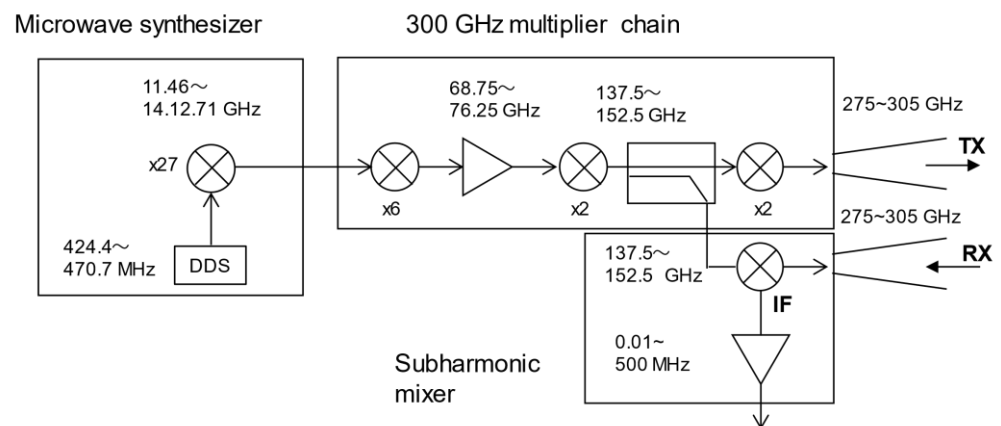

Figure 4. Schematic of 300 GHz FM-CW radar.

2.3. Optical Designing and Configuration

This section discusses the optics of the body scanner system. First, the overall configuration of the optical system was carefully examined from the design stage. In order to ensure uniform measurements even when the depth position of the pedestrian changes, it is necessary to ensure that the beam size of both the illuminated and detected beams does not change with position. For this purpose, both beams must propagate in the same direction. Therefore, constructing an optical system that separates both beams would result in a very large optical system, and significantly reduce the efficiency of irradiation beam utilization. Such a large system also becomes difficult to stack for future use. For these reasons, we had decided to use a beam splitter (BS) to share the identical beam direction for both systems. Although there is a loss of signal when BS is inserted, we have evaluated the S/N ratio as described above and determined that it does not have a significant impact on the measurements. Thus, we have decided to introduce the BS in our optics.

Next, the actual optics of the body scanner system is described. The Tx signal was used as an illumination beam to the target, and the returned signal from the target was introduced into the Rx as shown in Figure 5. For the optics, the illumination and scanning optics were separated to prevent stray light from the Tx side from mixing with the Rx side.
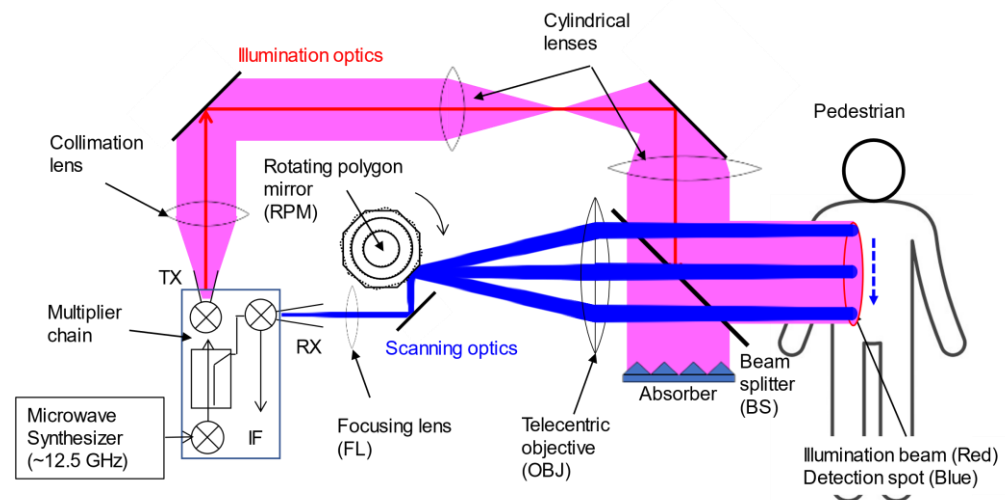
Figure 5. Schematic of the optical system.

The illumination and scanning optical paths were coaxialized by a BS located away from the transceiver. In the illumination optics, the Tx beam was circularly collimated with a collimating lens and vertically spread with a cylindrical lens paired to an elliptical collimated beam. It was then reflected by the BS and irradiated to the target.

The reflected or scattered beam from the target passes through the BS, and enters the telecentric objective lens (OBJ) and the Rx through the 8-plane rotating polygon mirror (RPM) and focusing lens (FL). The telecentric OBJ is particularly important in this optical design. The introduction of the lens ensures that the main beam is often parallel to the optical axis of the lens even when the receiving beam is scanned in the vertical direction, enabling the acquisition of 3D images without depth-dependent lateral distortion. All lenses used on these optics were made of high-density polyethylene (HDPE).

In designing the optics, depth of focus (DOF) and spot size were considered important. This is because a long DOF is necessary to measure a pedestrian at an oblique 45° angle, and a smaller beam size provides better image resolution. In this design, the optical system was treated as a Gaussian optical system, and the DOF was defined as twice the Rayleigh range. The DOF or Rayleigh range z_0 is given as follows:

$$\text{DOF} = 2z_0 = \frac{2\pi f}{c}(2\sigma_0)^2 = \frac{\pi f}{c}\frac{d_0^2}{\ln 2} \tag{4}$$

where f is the frequency of the radiation. σ_0 corresponds to a sigma value of the Gaussian profile at beam waist and diameter or detection spot, defined as the full width of half maximum (FWHM) d_0, given by $d_0 = 2\sqrt{2\ln 2}\,\sigma_0 = 2.35\,\sigma_0$.

As presented in Equation (4), there is a trade-off between DOF and d_0, and a longer DOF results in a larger beam diameter. To solve this trade-off, we focused on the selection of f. Equation (4) indicates that the higher the frequency, the longer DOF can be obtained while maintaining a small beam diameter d_0. However, the upper limit of frequency available to the body scanner is determined by the transparency of the cloth fiber. The transmission of many fibers decreases with increasing frequency, and the attenuation is greater than 3 dB at frequencies higher than 300 GHz [14]. Therefore, 300 GHz was adopted in this system because the attenuation is less than 3 dB for typical fibers and has the shortest wavelength. In the actual design, d_0 was 10.5 mm for f = 300 GHz and DOF = 500 mm. Furthermore, even for the entire DOF, the beam diameter range was 10.5–14.8 mm, providing sufficient spatial resolution for the inspection of concealed objects. The numerical aperture (NA) of the detection optics was 0.036 based on this DOF and spot size.

In the lens shape design, telecentricity, which affects the degree of depth-dependent lateral distortion of the 3D image, was primarily considered. To obtain high telecentricity, Optic Studio (Zemax) optical design software was used to optimize the lens shape. The diagonal horn antennas used for the receiver and transmitter were designed such that more than 80% of the radiated energy is a Gaussian beam in the TEM_{00} mode [15], thus it was possible to perform such an optimization using Optic studio (Zemax). The shape and position of each lens were designed based on the reciprocal theorem, assuming that the receiving beam follows the same optical path as the beam emitted from the receiver antenna.

Figure 6 shows the configuration of the scanning optics and rays at different polygon mirror angles. The focal length of the OBJ was 370 mm. Its vertical effective diameter was 300 mm, and the width of the vertical scan was determined by this diameter.
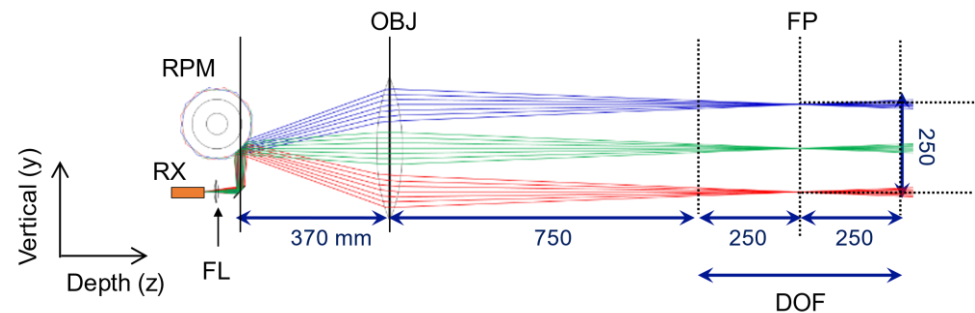

Figure 6. Ray of the scanning optical path.

The polygon mirror was positioned such that its reflection point was at the focal point of the telecentric lens. When the ray rotates 45° at this mirror position, the ray moves vertically 300 mm on the telecentric lens placed 370 mm away, and the detection spot at the target position also moves vertically 300 mm. Therefore, considering that the rotation angle of the polygon mirror is 1/2 of the rotation angle of the ray, the mirror should rotate 22.5° to vertically scan 300 mm. Because the center angle of each of the 8-sided polygon mirrors is 45°, only half the rotation angle contributes to scanning the detection spot. Rotation of this polygon mirror at 1065 rpm of rotation speed results in a vertical beam scan of 142 lines/s. Thus, to measure 200 pixel data points per single vertical scan within a time equivalent to 22.5° of mirror rotation, the radar measurement should be taken at 17 μs per pixel.

In these optics, in addition to the telecentric lens, an FL with a focal length of 51 mm was introduced to focus the ray at 1 m from the main plane of OBJ to achieve DOF = 500 mm and d_0 = 10.5 mm at 300 GHz as shown previously.

The size of one face of the polygon mirror is another factor that limits spatial resolution. That is, if the solid angle of one side of the mirror viewed from the waveguide of the Rx in Figure 6 is smaller than the radiation angle of the antenna, then the spot size at the target becomes larger because of the diffraction limit. Therefore, the size of one mirror face was set to 60 × 40 mm, and the diameter of the polygon mirror to 156 mm, to ensure a sufficient field of view at any given angle of the mirror.

2.4. Data Processing

In this system, measurements were automatically taken while the pedestrian passed through GS1 and GS2, and finally, a 3D image was displayed on the display. These series of signal processing were controlled using a field-programmable gate array (FPGA)-based real-time data processing system (DPS) developed by 3D Innovation Co. Ltd., Sendai, Japan. Figures 7 and 8 show the wiring diagram and measurement flowchart, respectively. When the GS1 detects the passage of a pedestrian, a start trigger is sent to the DPS. Triggered by this signal, the DPS starts acquiring the rotation encoder and index signals from the motor driver of the polygon mirror scanner. Based on the encoder signal, it sends a frequency-sweep start trigger to the synthesizer and acquires the IF signal output from the transceiver. This series of frequency sweep and data acquisition continues until the pedestrian passes

GS2 and the DPS receives a stop trigger. Until the completion of this passage, the DPS automatically extracts the reflection intensity and depth information by performing fast Fourier transform (FFT) processing based on the FM-CW radar principle and transfers the results to a PC through the ethernet with parallel processing.
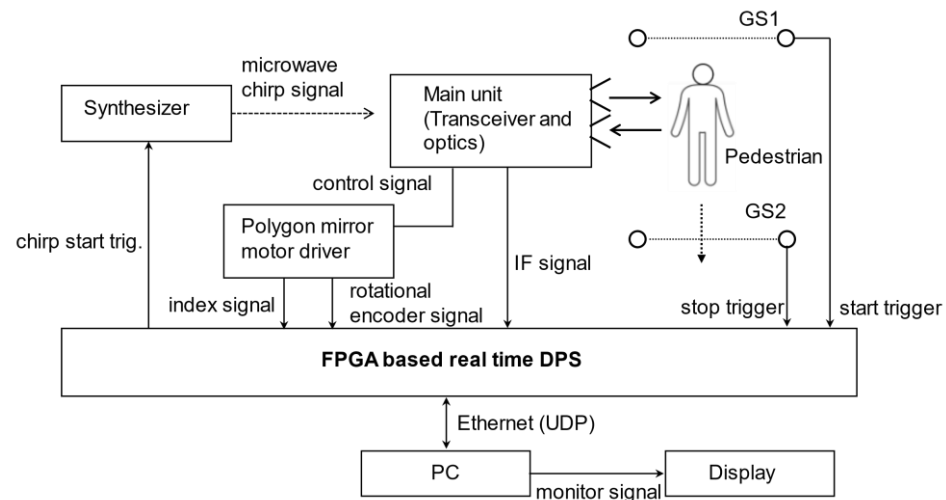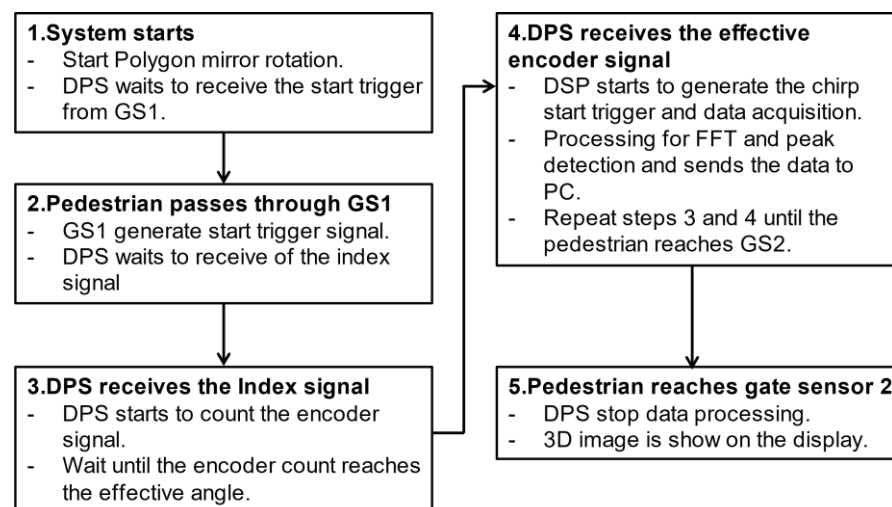

Figure 7. Block diagram of walk-through body scanner.

Figure 8. Flow of data acquisition.

Figure 9 shows the timing chart of the trigger signals from GS1 and GS2, the polygon mirror index trigger, and mirror rotation angle when passing through GS1 and GS2. The polygon mirror motor driver generates an index signal for every revolution and an encoder signal every 0.1125°. During the measurement, the polygon mirror rotates 20–30 times depending on the walking speed, and the number of rotations is shown as n^{th} in the figure. The bottom row shows the angle of rotation of the polygon mirror, and the gray area is when the DPS performs the radar measurements. This corresponds to when the RX can detect the beam passing through the telecentric lens from the target side using the polygon mirror. Thus, as aforementioned, 50% of the actual measurement time is available for data acquisition.
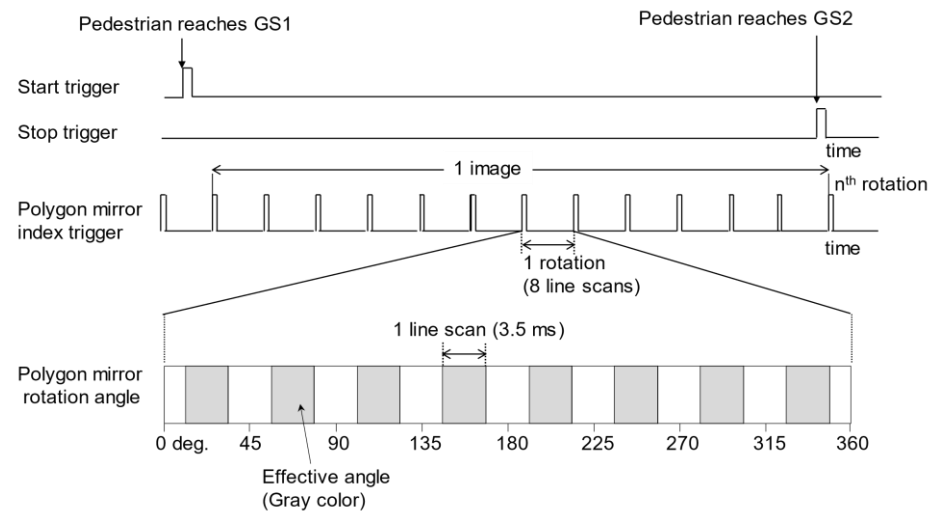
Figure 9. Timing chart for the acquisition of an image.

Figure 10 shows a timing chart during one vertical scan period, corresponding to one gray area in the bottom row in Figure 9. The top row is the chart for the encoder pulse and sweep start trigger, demonstrating the same waveform. As the DPS constructs one pixel for each pulse of the encoder signal, it takes 3.4 ms to measure one line consisting of 200 pixels. The second row shows the slope of the frequency sweep from 275 to 305 GHz. The sweep duration is 10 μs, and the following 7 μs are used for zero-filling and data processing, during which the frequency sweep is stopped. The third row is the waveform of the IF signal digitized by a 14-bit A/D converter (AD9680, Analog Devices Inc., Wilmington, NC, USA) with a concatenated zero value. This dataset consists of 2500 point IF signals followed by 1596 zero value points, for a total of 4096 data points. The zero-filled IF signal data are finally multiplied by the window function as shown in the fourth row in the figure, and FFT processing is performed in parallel with data acquisition to convert it into a range (depth) profile consisting of 2048 points. According to Nyquist's theorem, the maximum frequency of the spectrum is 125 MHz, corresponding to 12.5 m in terms of optical path length.
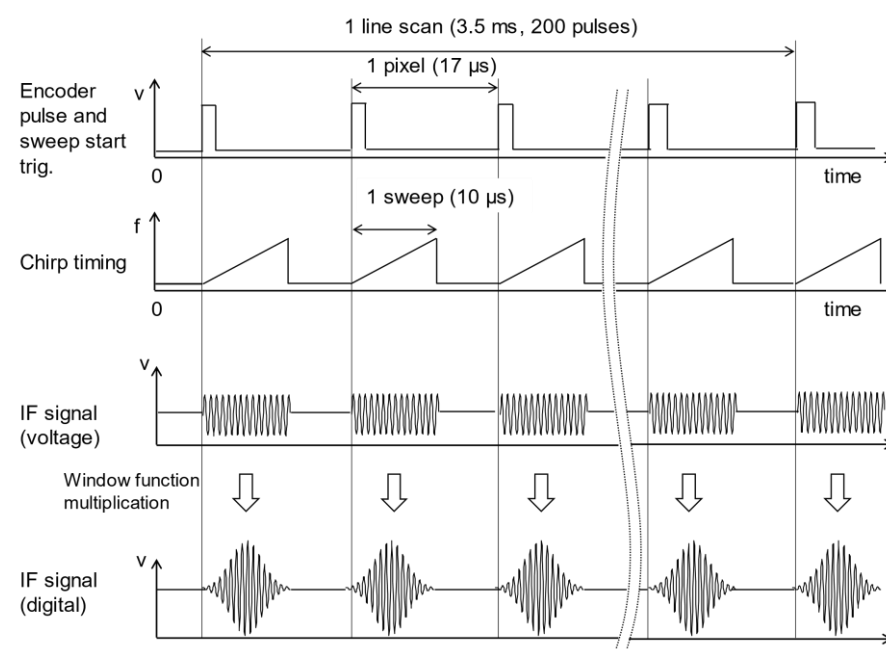

Figure 10. Timing chart during a vertical scanning and data processing.

The DPS also performs data processing to create 3D images. Using the range profile data, it extracts the signal intensity and distance information for peaks appearing within 1.5–2.5 m of the transceiver for up to 8 peaks. The vertical detection position converted from the encoder signal of the polygon mirror is then added to the above data to obtain the data for a single measurement point. These data concerning the 1D depth direction are accumulated for eight vertical lines and transferred to the control PC as a single packet. Based on this information, the 3D image is reconstructed by the PC. The time required to display the 3D image after a pedestrian passes through GS2 is approximately 0.4 s; however, this is mainly the time for the 3D display in LabVIEW, and it can be reduced using a graphics processing unit (GPU).

3. Results and Discussion

First, the measurement results of the illuminated beams were evaluated. Figure 11 shows the beam profiles measured at positions 500 mm, 750 mm, and 1000 mm from the BS. The measurements were performed by obtaining the intensity distributions by scanning a DLATGS (Deuterated L-Alanine Triglycine Sulfate) pyroelectric detector with the detection area of 3 mm in diameter. As can be seen from them, the beam sizes were 255–260 mm (FWHM) in the vertical direction and 38–46 mm (FWHM) in the horizontal one. Thus, the beam shapes were almost identical to each other, and we confirmed that the collimated beam along with the optical design was realized.
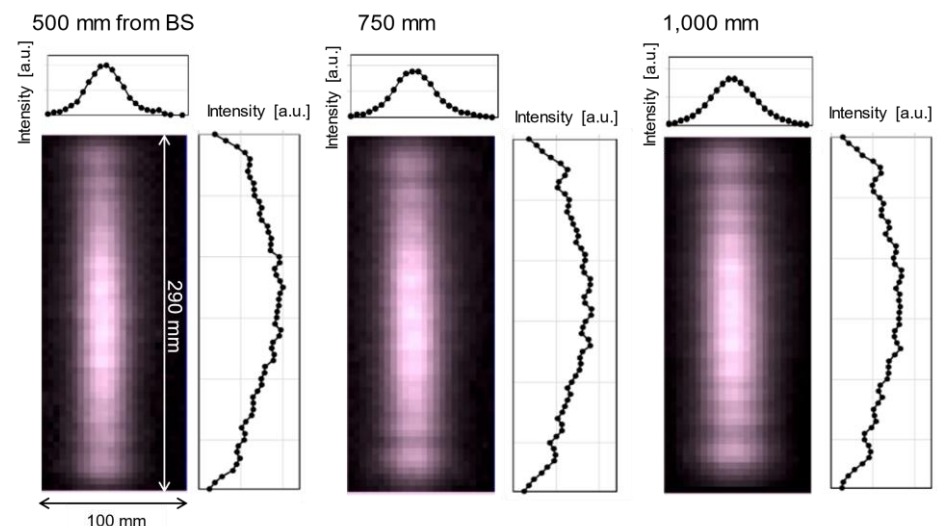

Figure 11. The illuminated beam profiles measured at 500 mm, 750 mm, and 1000 mm apart from the beam splitter.

The key parameters that characterize the quality of 3D images in this system are the spot sizes of the detection beams, FM-CW radar resolution, and telecentricity. The relationship between beam size and depth position was measured to evaluate the lateral spatial resolution and DOF. The images were acquired by scanning a 10 mm diameter metal sphere in a lateral 2D plane. For this, a 10 mm diameter metal sphere was scanned in the lateral 2D plane to obtain 3D data, and they were reconstructed into 2D images. Then, Gaussian fitting was applied to the vertical and horizontal cross-sectional profiles to derive the detection spot size. Figure 12a shows the horizontal and vertical detected spot sizes along the optical axis. As shown in the 2D image example in the inset of the figure, the reflection image of the metallic sphere was circular, and the sizes of the horizontal and vertical beams were almost identical within a distance of 500 mm. The spot size was smallest near the focal point and its range was 10.2–13.3 mm over the distance. Thus, it was confirmed that the spot size characteristics of the detection beam were in good agreement with the optical design.
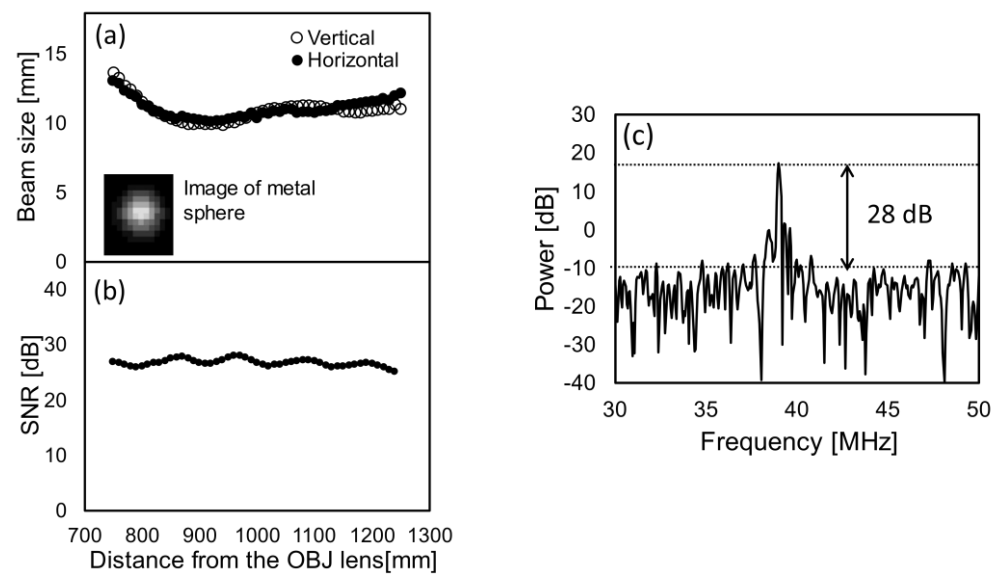
Figure 12. (**a**) Detection of spot size and (**b**) sensitivity variation with the optical direction. (**c**) Power spectra of a radar signal from a metal sphere located near focus.

Next, to evaluate the relationship between depth position and detection sensitivity, the signal-to-noise ratio (SNR) was measured. Figure 12b shows the plot of the SNR along the optical axis when a metal sphere was used as the target. The maximum SNR was measured near the beam waist, and it slightly decreased with increasing distance from the waist; however, the decrease was less than 3 dB. Figure 12c shows the range profile when a metal sphere was placed near the focal point, and the SNR was defined as the ratio of the peak height to the noise floor. The maximum SNR was 28 dB observed near the focal point.

In 3D imaging, the depth-dependent lateral distortion affects the reproducibility of 3D image reconstruction. To evaluate this effect, the images obtained at each depth position were compared. As shown in the photograph in Figure 13, a target consisting of three metal spheres 10 mm in diameter equally spaced vertically was used. The target was moved from 750 mm from the objective lens in 50 mm increments, and the image measurements were taken. For vertical scanning, the detection spot was scanned by rotating the polygon mirror, while the horizontal scanning was performed by placing the sample on a single-axis automated stage.
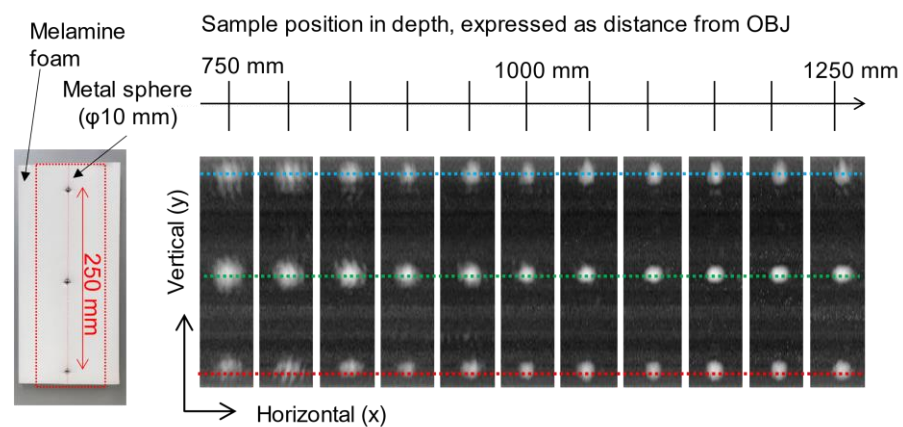

Figure 13. Reflected images of three metal spheres at different distances on the optical axis.

The grayscale images in Figure 13 are images with different depth positions of the target. The three white circles aligned vertically are metal spheres, and the spacing between the three conductor spheres is equal in all images. Thus, it was confirmed that the depth-

dependence of lateral distortion could be reduced using an optical system with high telecentricity and optical system that reproduces the three-dimensional structure of a pedestrian even when measuring from an oblique direction.

Next, we evaluated depth resolution, one of the most important parameters related to the detection performance of concealed objects. In this measurement, a shirt was stretched flat, and a metal sphere 10 mm in diameter was placed behind it. The target was placed at a distance of 1 m from the OBJ and the range profiles were measured by moving the distance between the shirt and the sphere by 30 mm in 10 mm increments from 0 mm. The depth resolution was defined as the FWHM of the peak at which the shirt and sphere could be separated by the radar. Figure 14 shows the range profiles obtained at different distances between the shirt and the sphere. The FWHM of the peak from the reflected signal from the sphere was 7 mm as shown in the figure, approximately 40% larger than the resolution calculated from the FM-CW principle.
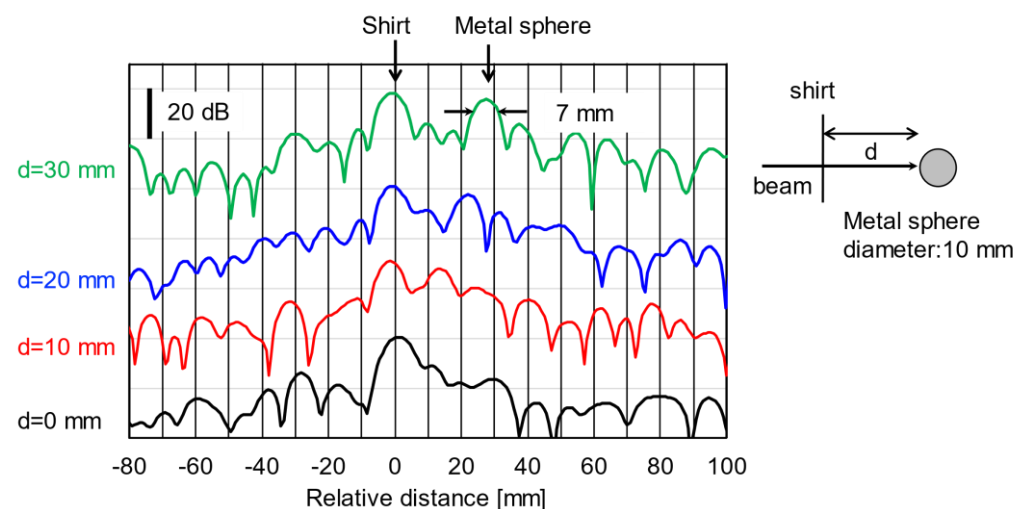

Figure 14. Range profile (power spectra) of a stretched shirt in front of a metal sphere at various separations.

Finally, 3D image measurements of a pedestrian with a bag containing a plastic model gun hidden under his clothing were performed to verify the detection performance of the concealed object. Figure 15a shows the actual measurement. In this experiment, the pedestrian wore cotton underwear, a thick long-sleeved shirt with a collar, and a polyester wool jacket. The bag containing the plastic model gun was concealed under the jacket. As shown in Figure 15a, the dimensions of the model gun were 115 mm × 150 mm and approximately 30 mm thick. The gun was held at a distance of approximately 50 mm from the body surface. Figure 15b,c shows the 3D images with and without the bag. In Figure 15c, the shape of the gun inside the bag was recognizable. Simultaneously, the scattered signals from the bag were received. The walking speed derived from the transit time between two gate sensors and their distance was approximately 4 km/h.

Figure 16 shows the results of a demonstration of detection of threats hidden in pockets. In this experiment, 3D images were measured when a pedestrian put only his hand in his pocket and he held a model gun in his pocket. Figure 16a,b shows the results of 3D images measured under each condition. The model gun appeared in the 3D image as shown in Figure 16b. These figures are captured images displayed on the monitor just after pedestrians passed through GS2. Thus, it has become clear that this system is suitable for rapid security screening in crowded places such as event venues because it can display data in real time without performing post-analysis after data acquisition.
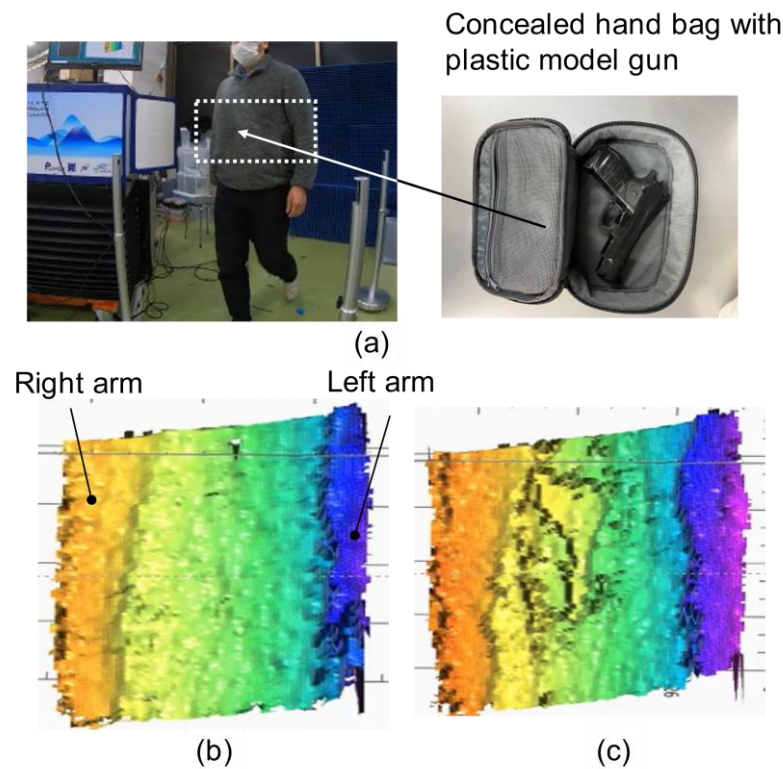
Figure 15. (**a**) Target scenario of a pedestrian concealing a handbag containing a model gun. (**b**,**c**) 3D reconstruction images of a pedestrian with and without handbag containing a plastic model gun.
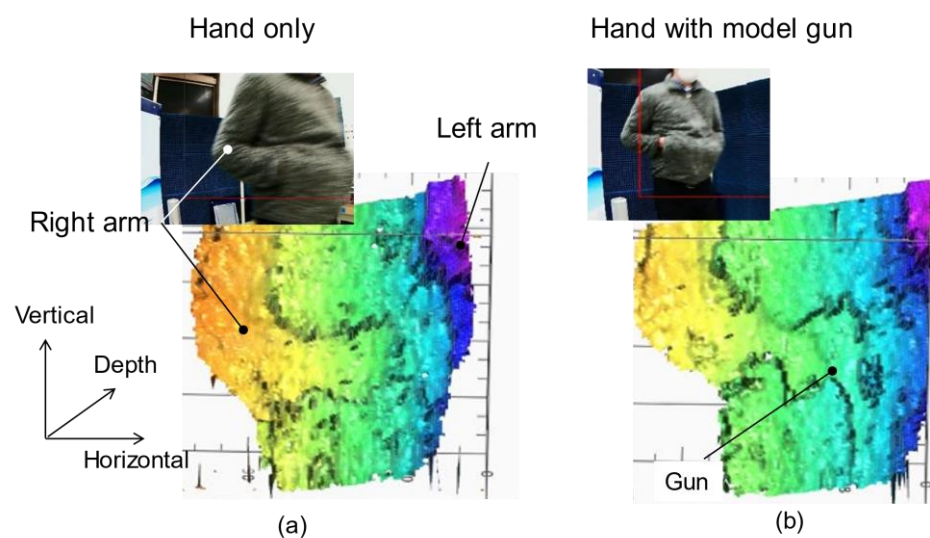

Figure 16. (**a**) 3D image measured with only the hand in the pocket. (**b**) 3D image measured by holding a model gun in the pocket.

We also confirmed that the gun could be recognized in the 3D image during the measurement even when walking at 7 km/h, 1.75 times faster than the above measurements. In this walking test, pedestrians passed between the gates as if they were actually walking down the passageway, without any special consideration for their movements. The 3D image of the concealed object was reconstructed under realistic walking conditions, demonstrating the proof-of-concept of the system.

As shown in this experiment, the measurement results obtained were used as they were and displayed as 3D images. However, in an actual usage environment where dis-

crimination will be performed for a large number of pedestrians, automatic discrimination by software will be required instead of human judgments. To address this issue, it would be effective to develop algorithms that utilize 3D analysis technology such as that applied to tomographic imaging.

To expand the measurement area using multiple units as shown in Figure 1, it is necessary to avoid crosstalk between units. Time-divided operation of each unit will be effective to solve this problem. With the current unit, the radar measurement time accounts for approximately 30% of the 3D image measurement time. Reducing the sweep time from 10 µs to 8 µs can reduce that ratio to 25%, and a time-division scheme will allow four units to operate simultaneously without crosstalk.

Moreover, it would be also useful to measure both the front and back of a pedestrian using two beam paths that are split by a beam splitter. In this unit, one beam was split by the beam splitter and the other beams were blocked by an absorber as shown in Figure 5. However, the back of the human body could be measured using the beam on the absorber side. We experimentally confirmed that this method works effectively. By combining these improvements, it is expected that a whole-body inspection of pedestrian can be eventually realized with the system shown in Figure 1.

4. Conclusions

In this study, we report on the development and characterization of a terahertz wave-radar 3D imaging system for realizing a walk-through security gate. In the system, the number of scans was reduced by walking motion to move the detection spot horizontally, and the concealed objects carried by pedestrians moving at a speed of approximately 4.0 km/h were successfully visualized. Imaging measurements with actual walking movements showed that pedestrians did not require any special care in their walking movements, and the 3D images of concealed objects were clearly visible if they passed through the gate as if they were normally walking on a sidewalk. To the best of our knowledge, this is the first example of active 3D sub-THz radar-imaging visualizing concealed objects carried by a pedestrian moving at a realistic walking speed of up to 7 km/h.

In our system, high-speed 3D imaging was achieved with a single-element transceiver, assuming that an inexpensive system can be achieved soon. The transceiver used here is conventional, which uses a multiplier chain based on Schottky barrier diode technology, but when semiconductor chip-type transceivers are realized with the advancement of B5G/6G technology, a tremendous reduction in cost and size of components is expected [16,17]. Furthermore, the introduction of high-capacity wireless communication technology will enable analysis processing by a central server, eliminating the need for a signal processing system for each unit. By reducing the size and weight of the optical system, the system can be combined with a mobile robot. With these technological advancements, a compact and inexpensive system can be realized soon, which will be the cornerstone of this technology.

Conflicts of Interest: The authors declare no conflict of interest.

References

1. Cooper, K.B.; Dengler, R.J.; Llombart, N.; Bryllert, T.; Chattopadhyay, G.; Schlecht, E.; Gill, J.; Lee, C.; Skalare, A.; Mehdi, I.; et al. Penetrating 3-D Imaging at 4- and 25-m Range Using a Submillimeter-Wave Radar. *IEEE Trans. Microwave Theor. Tech.* **2008**, *56*, 2771–2778. [CrossRef]

2. Wang, Z.; Chang, T.; Cui, H.-L. Review of active millimeter-wave imaging techniques for personnel security screening. *IEEE Access* **2019**, *7*, 148336–148350. [CrossRef]

3. Robertson, D.A.; Macfarlane, D.G.; Hunter, R.I.; Cassidy, S.L.; Llombart, N.; Gandini, E.; Bryllert, T.; Ferndahl, M.; Lindström, H.; Tenhunen, J.; et al. High resolution, wide field of view, real-time 340 GHz 3D imaging radar for security screening. In *Proceedings of the SPIE*; SPIE: Anaheim, CA, USA, 2017; Volume 101890C. [CrossRef]

4. Cooper, K.B.; Dengler, R.J.; Chattopadhyay, G.; Schlecht, E.; Gill, J.; Skalare, A.; Mehdi, I.; Siegel, P.H. A high-resolution imaging radar at 580 GHz. *IEEE Microw. Wirel. Compon. Lett.* **2008**, *18*, 64–66. [CrossRef]

5. Sheen, D.M.; Hall, T.E.; Severtsen, R.H.; McMakin, D.L.; Hatchell, B.K.; Valdez, P.L.J. *Standoff Concealed Weapon Detection Using a 350-GHz Radar Imaging System*; SPIE Proceedings: San Diego, CA, USA, 2010; p. 767008. [CrossRef]

6. Cooper, K.B.; Dengler, R.J.; Llombart, N.; Talukder, A.; Panangadan, A.V.; Peay, C.S.; Mehdi, I.; Siegel, P.H. *Fast High-Resolution Terahertz Radar Imaging at 25 Meters*; SPIE Proceedings: San Diego, CA, USA, 2010; p. 76710Y. [CrossRef]

7. Cooper, K.B.; Dengler, R.J.; Llombart, N.; Thomas, B.; Chattopadhyay, G.; Siegel, P.H. THz imaging radar for standoff personnel screening. *IEEE Trans. Terahertz Sci. Technol.* **2011**, *1*, 169–182. [CrossRef]

8. Sheen, D.M.; McMakin, D.L.; Hall, T.E. Active millimeter-wave and submillimeter-wave imaging for security applications. In Proceedings of the 2011 36th International Conference on Infrared, Millimeter, and Terahertz Waves (IRMMW), Houston, TX, USA, 2–7 October 2011; pp. 1–3. [CrossRef]

9. Cooper, K.B. Performance of a 340-GHz radar transceiver array for standoff security imaging. In Proceedings of the 2014 39th International Conference on Infrared, Millimeter, and Terahertz Waves (IRMMW), Tucson, AZ, USA, 14–19 September 2014. [CrossRef]

10. Sasaki, Y.; Ikari, T.; Otani, C. Development of body scanner in the terahertz region using the FMCW method. *IEICE Tech. Rep.* **2019**, *119*, 61–64. (In Japanese)

11. Otani, C.; Ikari, M.; Sasaki, Y. *Development of 300 GHz Walk-Through Body Scanner for the Security Gate Applications*; SPIE Proceedings: Anaheim, CA, USA, 2021; p. 118270N. [CrossRef]

12. Ikari, T.; Sasaki, Y.; Otani, C. Development of Terahertz walk-through body scanner using 300 GHz FMCW radar. In Proceedings of the 2022 47th International Conference on Infrared, Millimeter, and Terahertz Waves (IRMMW), Delft, The Netherland, 28 August–2 September 2022. [CrossRef]

13. Otani, C.; Ikari, T.; Sasaki, Y. Terahertz imaging with frequency modulated continuous wave (FMCW) radar the review of laser. *Engineering.* **2022**, *50*, 468–472. (In Japanese)

14. Bjarnason, J.E.; Chan, T.L.J.; Lee, A.W.M.; Celis, M.A.; Brown, E.R. Millimeter-wave, terahertz, and mid-infrared transmission through common clothing. *Appl. Phys. Lett.* **2004**, *85*, 519–521. [CrossRef]

15. Johansson, J.F.; Whyborn, N.D. The diagonal horn is a submillimeter wave antenna. *IEEE Trans. Microw. Theor. Tech.* **1992**, *40*, 795–800. [CrossRef]

16. Hillger, P.; Grzyb, J.; Jain, R.; Pfeiffer, U.R. Terahertz imaging and sensing applications with silicon-based technologies. *IEEE Trans. Terahertz Sci. Technol.* **2019**, *9*, 1–19. [CrossRef]

17. Fujishima, M. Future of 300 GHz band wireless communications and their enabler, CMOS transceiver technologies. *Jpn. J. Appl. Phys.* **2021**, *60*, SB0803. [CrossRef]